Optical microscope for three-dimensional surface displacement and shape measurements at the microscale

Shuman Xia,* Zhipeng Pan, and Jingwen Zhang

Woodruff School of Mechanical Engineering, Georgia Institute of Technology, Atlanta, Georgia 30332, USA
**Corresponding author: shuman.xia@me.gatech.edu*

Received December 30, 2013; accepted May 26, 2014;
posted June 10, 2014 (Doc. ID 203862); published July 15, 2014

We report a novel optical microscope for full-field, noncontact measurements of three-dimensional (3D) surface deformation and topography at the microscale. The microscope system is based on a seamless integration of the diffraction-assisted image correlation (DAIC) method with fluorescent microscopy. We experimentally demonstrate the microscope's capability for 3D measurements with submicrometer spatial resolution and subpixel measurement accuracy. © 2014 Optical Society of America

OCIS codes: (120.0120) Instrumentation, measurement, and metrology; (180.6900) Three-dimensional microscopy; (050.0050) Diffraction and gratings; (100.2000) Digital image processing.
http://dx.doi.org/10.1364/OL.39.004267

The use of optical techniques in three-dimensional (3D) surface deformation and profile analyses offers several compelling advantages, such as noncontact operation, full-field measurement capability, and fast data acquisition. Driven by various industrial needs as well as research in biology and materials science, there is a growing interest in performing such analyses at the micro- and nanoscales. Good cases in point include warpage inspection of microelectronics components [1], mechanobiological study of cells and tissues [2], and micromechanical test for thin-film characterizations [3].

There are a range of optical techniques currently in use for measuring height profiles and displacements in 3D. Some of the commonly used full-field profiling methods include white-light and laser interferometry [4], projection Moire interferometry [5], depth from focus/defocus (DFF/DFD) [6–8], as well as 3D digital image correlation (3D-DIC) [9,10]. A small number of approaches are available for 3D full-field displacement measurements. Among them, 3D electronic speckle pattern interferometry (ESPI) [11] offers the highest measurement sensitivity (down to a few nanometers) but suffers from very limited measurement range due to speckle decorrelation. On the other hand, 3D-DIC is capable of characterizing large displacements with subpixel measurement accuracy.

Despite the advent of the above measurement techniques, high-accuracy optical 3D deformation and profile characterizations at the microscale remain a great challenge. There have been several studies that have combined 3D-DIC with stereomicroscopy to enable 3D measurements at small length scales. Sutton *et al.* [12] for the first time developed a stereo-microscopic 3D-DIC system and used it for strain-field measurements of mouse carotid arteries. A similar 3D fluorescent stereo microscope was developed by Hu *et al.* [13] and tested via topography and surface deformation measurements of a biofilm. The spatial resolution of these microscopic 3D-DIC systems has been limited to a few micrometers due to the low magnification power of stereomicroscopy. Traditional compound microscopes can achieve submicrometer spatial resolution, but they are only capable of two-dimensional (2D) imaging. In a recent study, Li and Yi [14] developed a freeform prism array that could be attached to the objective of a microscope to enable 3D stereo imaging. They demonstrated the viability of their method through qualitative 3D imaging tests but did not provide a viable route for quantitative 3D shape reconstruction.

Xia and co-workers [15,16] have recently developed a novel image correlation-based technique, named diffraction-assisted image correlation (DAIC), for 3D full-field deformation and profile measurements. The DAIC method utilizes a transmission grating and a single camera to achieve 3D perception, making it particularly suitable for microscopic applications. In this Letter, we present a novel 3D microscope that has been newly developed by seamlessly integrating the DAIC technique with a compound optical microscope. The microscope has a unique capability of 3D deformation and morphology measurements with submicrometer spatial resolution.

Figure 1 shows the schematic and actual experimental setup of the 3D microscope system. The layout of the microscope closely resembles that of an epi-illuminated fluorescence microscope. Two infinity-corrected microscope objectives (objectives 1 and 2) (Nikon CFI Plan Apo 20×, N.A. 0.75 and Olympus UPlanFL N 20×, N.A. 0.50) are placed back-to-back and are used to form an intermediate real image (P') of a micro-sized specimen (P). A custom-made transmission diffraction grating (Ibsen Photonics, Denmark) is positioned right above the real image. The grating has a constant line spacing of 2000 nm, and a rectangular profile specially designed to suppress the zeroth-order light diffraction. The ruling of the grating is aligned with the y-direction. Therefore, diffraction by the transmission grating along the x-direction creates two first-order virtual images corresponding to the intermediate real image. A third microscope objective (objective 3, Nikon BD Plan 20×, N.A. 0.4) is used to project the virtual images onto the sensor plane of a high-resolution, Peltier-cooled CCD camera (ML8300M, Finger Lakes Instrumentation, Lima,

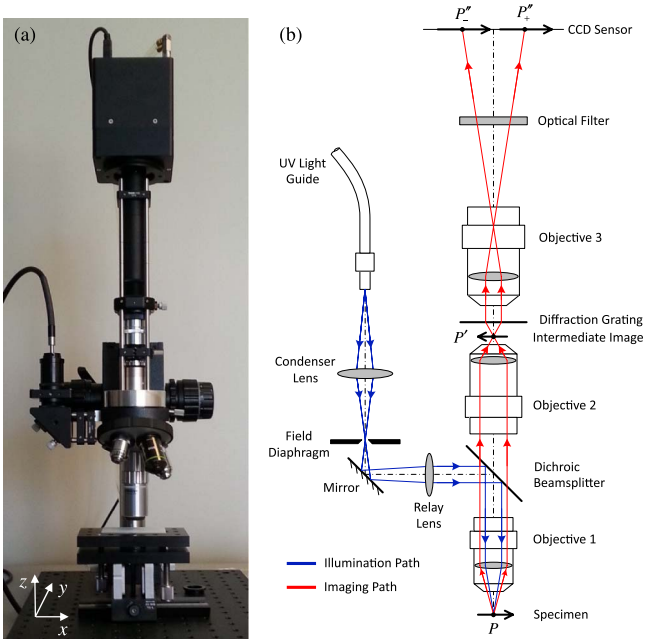

Fig. 1. (a) Photograph of the newly developed optical microscope for three-dimensional (3D) surface displacement and profile measurements and (b) schematic layout of the microscope.

New York) with 16-bit digital digitization. The pixel scale of the final projected image is 0.53 μm/pixel.

Illumination of the specimen is provided by an ultraviolet (UV) light-emitting diode (LED) light source. An iris field diaphragm is positioned in the illumination path so the size and location of the illuminated area can be precisely controlled. A 450 nm filter with 10 nm bandpass is inserted in the imaging path, to filter out the background light as well as to suppress chromatic dispersion of the grating. The entire setup is placed on a vibration isolation table to reduce external vibrations.

The 3D surface displacement or profile of the specimen is encoded in the projected first-order images (P''_- and P''_+). Decoding of such 3D data requires 2D full-field displacement analysis of the first-order diffracted images. In the present work, this analysis is carried out using the 2D digital image correlation (DIC) method [17,18]. The DIC method is based on the quantitative comparison of two high-contrast speckle images through cross-correlation coefficient maximization. In this work, a random speckle pattern required for the implementation of DIC is created by coating the specimen surface with fluorescent microparticles.

The 3D displacements of the specimen (P) and its intermediate image (P') are assumed to be related according to the following linear relationship:

$$u_{p'} = M_{xy}u_p + \alpha_x(x - x_c)w_p, \tag{1a}$$

$$v_{p'} = M_{xy}v_p + \alpha_y(y - y_c)w_p, \tag{1b}$$

$$w_{p'} = M_z w_p, \tag{1c}$$

in which M_{xy} and M_z are the in-plane and out-of-plane magnification factors, α_x and α_y are the coupling coefficients that account for the nontelecentricity of the imaging system, x_c and y_c are the coordinates of the center of perspective projection, (u, v) denote the in-plane displacements in the x- and y-directions, and w denotes the out-of-plane displacement in the z-direction. The 3D displacement of the intermediate image is further related to the in-plane displacements of the two first-order diffracted images (P''_- and P''_+) through [15]

$$u_{p''_-} = N_{xy}(u_{p'} + w_{p'} \tan\theta), \tag{2a}$$

$$u_{p''_+} = N_{xy}(u_{p'} - w_{p'} \tan\theta), \tag{2b}$$

$$v_{p''_-} = v_{p''_+} = N_{xy}v_{p'}, \tag{2c}$$

where N_{xy} is the magnification factor of objective 3 and θ is the first-order diffraction angle of the grating.

By substituting Eqs. (2a)–(2c) into Eqs. (1a)–(1c) and inverting the resulting equations, we obtain the 3D displacement of the specimen as

$$w_p = \frac{(u_{p''_-} - u_{p''_+})}{2N_{xy}M_z \tan\theta} = \beta_1 \frac{(u_{p''_-} - u_{p''_+})}{2}, \tag{3a}$$

$$\begin{aligned} u_p &= \frac{(u_{p''_-} + u_{p''_+})}{2N_{xy}M_z} - \frac{\alpha_x(x - x_c)}{M_{xy}} w_p \\ &= \beta_2 \frac{(u_{p''_-} + u_{p''_+})}{2} - \beta_3(x - x_c)w_p, \end{aligned} \tag{3b}$$

$$\begin{aligned} v_p &= \frac{(v_{p''_-} + v_{p''_+})}{2N_{xy}M_z} - \frac{\alpha_y(y - y_c)}{M_{xy}} w_p \\ &= \beta_2 \frac{(v_{p''_-} + v_{p''_+})}{2} - \beta_4(y - y_c)w_p. \end{aligned} \tag{3c}$$

Once the in-plane displacement fields of the two first-order diffracted views are obtained, the above equation can be used to calculate the 3D full-field displacement of the specimen. The free parameters of the optical system, $\beta_i (i = 1\text{–}5)$, can be calibrated against a known 3D displacement field.

The 3D profile measurement of a curved surface involves determining the surface height, h, as a function of in-plane coordinates, x_p and y_p. To derive a governing equation for profile measurement, we consider a virtual process in which the surface is initially flat and is deformed into the final curved shape with an out-of-plane displacement of $w = h$. Let $X_{p''_-}$ and $X_{p''_+}$ denote the initial x-coordinates of the first-order diffracted images and $x_{p''_-}$ and $x_{p''_+}$ denote the corresponding x-coordinates in the final configuration. According to Eq. (4), we have

$$\begin{aligned} w(x_{p''_-}, y_{p''_-}) &= \frac{\beta_1}{2}[(x_{p''_-} - X_{p''_-}) - (x_{p''_+} - X_{p''_+})] \\ &= -\frac{\beta_1}{2}u_{p''} + C, \end{aligned} \tag{4}$$

in which $u_{p''} = x_{p''_+} - x_{p''_-}$ is the relative displacement between the two first-order diffracted views in the final

configuration, and $C = \beta_1(X_{p''_+} - X_{p''_-})/2$ is the relative displacement in the initial configuration. Here, C is a constant, since the surface is made to be flat in the initial configuration. Then we map w from the coordinate space of the diffracted views to that of the specimen to obtain

$$h(x_p, y_p) = w\left(\frac{x_p}{\beta_2}, \frac{y_p}{\beta_2}\right) = -\beta_1 u_{p''}. \tag{5}$$

In writing the above equation, we have dropped the constant term, C. This causes a shift in the measured profile but does not affect the actual shape of the specimen. The full-field distribution of $u_{p''}$ can be measured by correlating the two first-order diffracted images with the 2D-DIC method, and Eq. (5) can then be used to obtain the surface profile of the specimen.

Rigid-body translation and rotation experiments were conducted to assess the validity of the 3D microscope system for displacement measurements. A flat-glass slide speckled with fluorescent particles was used as a test specimen. Figure 2 shows the negative and positive first-order diffracted views of a selected region on the glass slide. Note that the zeroth-order view, which corresponds to direct light transmission through the grating, does not show up due to strong intensity suppression of the zeroth-order diffraction.

In the rigid-body translation experiment, the glass slide was translated along the vertical (z) axis for 10.0 μm using a differential micrometer-driven translation stage. Four speckle images, including two negative first-order (−1st) images and two positive first-order (+1st) images, were captured before and after the rigid-body translation. The 2D-DIC analysis was carried out between the −1st-order images and between the +1st-order images, yielding two sets of displacement fields, ($u_{p''_-}$, $v_{p''_-}$) and ($u_{p''_+}$, $v_{p''_+}$), as shown in Fig. 3. Because light diffraction only acts in the x-direction, the two y-displacement maps are nearly identical. In contrast, the two x-displacement maps encode the out-of-plane displacement of the specimen in different ways, and therefore exhibit a large difference (note the difference in the displacement ranges). The specimen does not have any in-plane motion. However, all of the four displacement fields are linearly varying with similar gradients, indicating that the nontelecentricity of the microscope is significant.

The four displacement maps shown in Fig. 3 were used in Eqs. (3a)–(3c) to calculate the in-plane displacements (u_p, v_p) and out-of-plane displacement (w_p) of the specimen. The optical parameters in these equations were obtained by least-squares fitting the calculated

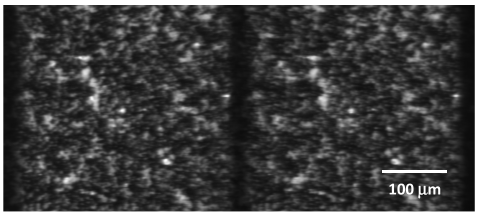

Fig. 2. Negative and positive first-order views of a speckle-patterned region on a flat-glass slide.

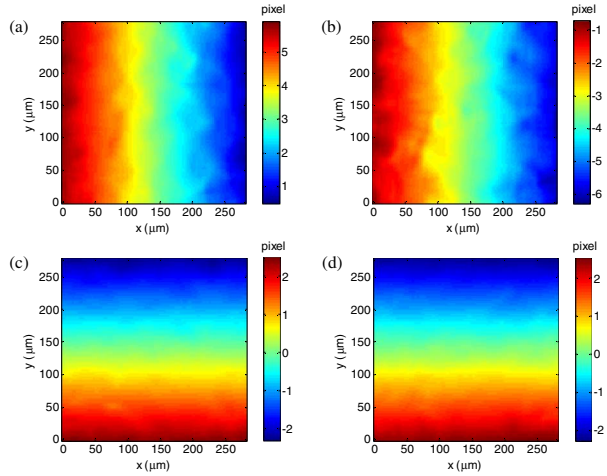

Fig. 3. In-plane displacement maps of the two first-order diffracted views due to an out-of-plane rigid-body translation of 10.0 μm: (a) negative first-order ($u_{p''_-}$), (b) positive first-order ($u_{p''_+}$), (c) negative first-order ($v_{p''_-}$), and (d) positive first-order ($v_{p''_+}$).

displacements to the actual imposed displacements. Figures 4(a)–4(c) shows the contour plots of the calculated in-plane and out-of-plane displacement components. The displacement profiles along the central horizontal line are plotted in Fig. 4(d).

To further demonstrate the measurement capability of the microscope, a second experiment was carried out in which the glass side was tilted about an axis along the y-direction for 6.0 deg using a rotation stage. The tilt produced constant in-plane displacement components and a linearly varying out-of-plane displacement field. Similar to the first experiment, four in-plane displacement components of the first-order diffracted views were obtained using 2D-DIC. The previously calibrated optical parameters were used to calculate the 3D displacements of the specimen from the current in-plane displacement maps. The obtained out-of-plane displacement is presented in Fig. 5(a). Figure 5(b) shows the measured 3D displacement profiles along the dashed section line in Fig. 5(a), together with the true out-of-plane displacement profile. The displacement in the x-direction

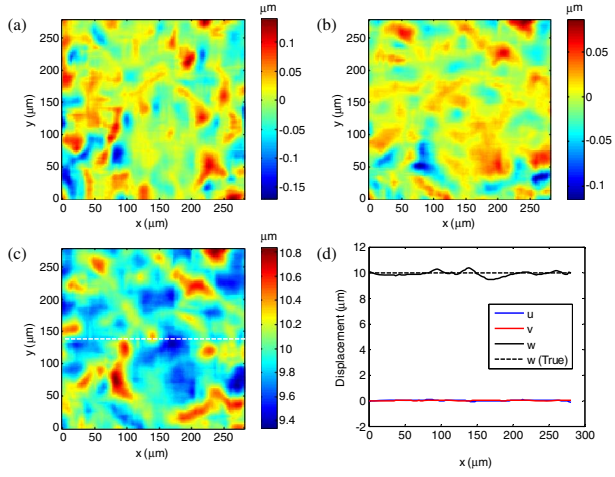

Fig. 4. Measured 3D displacement fields due to an out-of-plane translation of 10.0 μm: (a) u_p, (b) v_p, (c) w_p, and (d) displacement profiles along the dashed section line shown in (c).

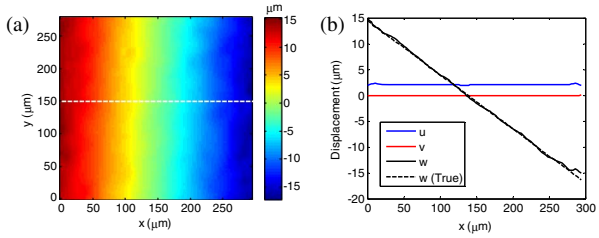

Fig. 5. (a) Measured z-displacement field due to an out-of-plane tilt of 6 deg and (b) displacement profiles along the dashed section line shown in (a).

(u) has a nonzero value of ~2 μm due to imperfect coaxiality of the rotation stage. The measured and true out-of-plane displacements compare favorably with each other.

The surface profiling capability of the microscope was tested by profiling the top surface of a steel ball (0.68 mm in diameter). The two first-order diffracted views of the test surface are shown in Fig. 6(a). The microscope was focused near the central region of the field of view. Hence, the perimeter of the field of view was noticeably out of focus. The central in-focused regions in the two diffracted views were correlated using the DIC method. The resulted x-displacement field was substituted in Eq. (5) to obtain the topography of the test surface as shown in Fig. 6(b). Comparison between the measured and true height profiles along two section lines is given in Fig. 6(c). A good level of agreement is found, especially near the central region of the field of view.

According to Eqs. (3a) and (5), the out-of-plane displacement (w_p) and profile (h) measurement errors scale linearly with the in-plane DIC measurement errors by a factor of β_1, which is inversely proportional to $\tan\theta$. Therefore, for improving the measurement accuracy of w_p and h, it is advisable to choose a maximum first-order diffraction angle allowed by the numerical apertures of the objectives.

Throughout the present investigation, the field of view for all the measurements is kept at about 300 μm. By changing the current 20× objective lens (objective 1) to a different magnification, one can vary the field of view and spatial resolution. It is worth pointing out that, by using a set of infinity-corrected objectives with the same parfocal length and different magnifications, the size and position of the intermediate real image (P') would remain unchanged as the magnification is changed. Therefore, there is no need to realign any optical components or refocus the microscope during switching of the objectives, which provides great convenience for performing multiscale measurements.

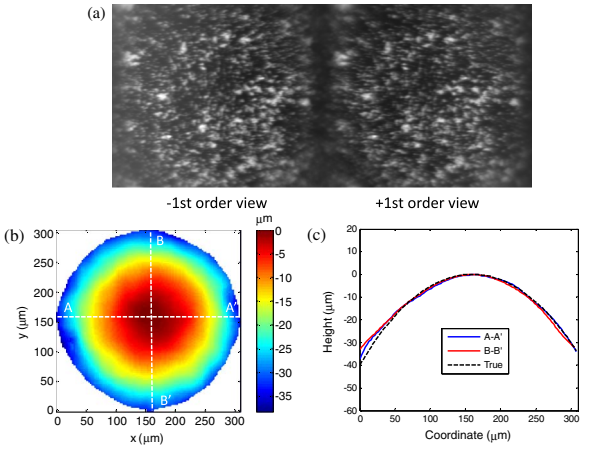

Fig. 6. (a) Negative and positive first-order views of a speckle-patterned spherical surface, (b) measured topography of the test surface, and (c) height profiles along the two dashed section lines shown in (b).

In conclusion, we have presented an optical microscope system for full-field, noncontact measurements of 3D surface deformation and topography at the microscale. The 3D microscope system was developed by a novel combination of the DAIC method and fluorescent microscopy. The theoretical basis for data analysis and processing was provided. The performance of the system was tested by measuring the 3D displacement components of rigid-body translation and rotation, as well as by profiling the top surface of a micro-sized ball. With the submicrometer spatial resolution and subpixel measurement accuracy demonstrated here, the 3D microscope can serve as a unique tool in biological and materials research, as well as in quality engineering and inspection.

We gratefully acknowledge a Haythornthwaite Research Initiation Grant administered through the Applied Mechanics Division (AMD) of the American Society of Mechanical Engineers (ASME).

References

1. S. Walwadkar, C. Kovalchick, W. Hezeltine, F. Liang, and A. McAllister, *Proceedings of the 2013 Annual Conference on Experimental and Applied Mechanics, MEMS and Nanotechnology* (Springer, 2013), Vol. **5**, pp. 23–31.
2. B. L. Boyce, J. M. Grazier, R. E. Jones, and T. D. Nguyen, Biomaterials **29**, 3896 (2008).
3. H. Espinosa, B. Prorok, and M. Fischer, J. Mech. Phys. Solids **51**, 47 (2003).
4. N. Balasubramanian, "Optical system for surface topography measurement," U.S. patent 4,340,306 (July 20, 1982).
5. W. Welford, Opt. Acta **16**, 371 (1969).
6. T. Darrell and K. Wohn, *Proceedings CVPR '88: The Computer Society Conference on Computer Vision and Pattern Recognition* (1988), pp. 504–509.
7. A. P. Pentland, Proc. IEEE Trans. Pattern Anal. Machine Intell. **9**, 523 (1987).
8. P. Grossmann, Pattern Recogn. Lett. **5**, 63 (1987).
9. P. Luo, Y. Chao, M. Sutton, and W. H. Peters, Exp. Mech. **33**, 123 (1993).
10. J. D. Helm, S. R. McNeill, and M. A. Sutton, Opt. Eng. **35**, 1911 (1996).
11. R. Jones, *Holographic and Speckle Interferometry* (Cambridge University, 1989).
12. M. Sutton, X. Ke, S. Lessner, M. Goldbach, M. Yost, F. Zhao, and H. Schreier, J. Biomed. Mater. Res. A **84**, 178 (2008).
13. Z. Hu, H. Luo, Y. Du, and H. Lu, Opt. Express **21**, 11808 (2013).
14. L. Li and A. Y. Yi, J. Opt. Soc. Am. A **27**, 2613 (2010).
15. S. Xia, A. Gdoutou, and G. Ravichandran, Exp. Mech. **53**, 755 (2013).
16. Z. Pan, S. Xia, A. Gdoutou, and G. Ravichandran, "Diffraction-assisted image correlation for three-dimensional surface profiling," Exp. Mech. (to be published).
17. W. Peters and W. Ranson, Opt. Eng. **21**, 427 (1982).
18. M. Sutton, W. Wolters, W. Peters, W. Ranson, and S. McNeill, Image Vision Comput. **1**, 133 (1983).